THERMAL ANALYSIS IN THIN-FILM FLUID REGIONS OF RECTANGULAR MICROGROOVE

by

Xiaohong GUI[a*], Xiange SONG[b], and Baisheng NIE[a]

[a] China University of Mining and Technology, Beijing, China
[b] Beijing International Studies University, Beijing, China

Original scientific paper
https://doi.org/10.2298/TSCI160114288G

The effects of contact angle and superheat on thin-film thickness and heat flux distribution occurring in a rectangle microgroove are numerically simulated. Accordingly, physical, and mathematical models are built in detail. Numerical results indicate that meniscus radius and thin-film thickness increase with the improvement of contact angle. The heat flux distribution in the thin-film region increases non-linearly as the contact angle decreases. The total heat transfer through the thin-film region increases with the improvement of superheat, and decreases as the contact angle increases. When the contact angle is equal to zero, the heat transfer in the thin-film region accounts for more than 80% of the total heat transfer. Intensive evaporation in the thin-film region plays a key role in heat transfer for the rectangle capillary microgroove. The liquid with higher wetting performance is more capable of playing the advantages of higher intensity heat transfer in thin--film region. The current investigation will result in a better understanding of thin--film evaporation and its effect on the effective thermal conductivity in the rectangle microgroove.

Key words: *contact angle, film thickness, heat flux distribution, rectangle microgroove*

Introduction

Rapid advances in the electronics industry have led to a great interest in high heat flux dissipation devices. Thin-film evaporation plays an important role in these modern highly efficient heat transfer devices [1, 2]. When thin-film evaporation occurs in the thin-film region, most of the heat transfers through a narrow area between the non-evaporation region and intrinsic meniscus region. The flow resistance of the vapor phase during thin-film evaporation is very small compared with the vapor flow in the liquid phase in a typical nucleate boiling heat transfer configuration. In addition, the superheat needed for the phase change in the thin-film region is much smaller than that for a bubble growth in a typical nucleate boiling, in particular, at the initial stage of the bubble growth. The heat transfer efficiency of thin-film evaporation is much higher than the nucleate boiling heat transfer. It is known that the thermodynamic properties of the liquid thin-film region are very different from those of the macroregion.

The thin-film evaporating region has been studied extensively by many investigators. Jiao *et al.* [3] developed a theoretical model predicting the heat transfer performance occurring in a grooved heat pipe. Li *et al.* [4] investigated the critical heat flux and evaporation rates from

* Corresponding author, e-mail: gxhbox@sina.com

capillary wicking structures. It was found that the critical heat flux depended heavily on the thickness of the capillary wick while the overall evaporation heat transfer was independent of wick thickness. Jiao *et al.* [5] also proposed an analytical model that could predict the effects of contact angle on the thin-film profile and meniscus radius within a micro trapezoidal groove. It was found that the thin-film evaporation governed the maximum heat transfer capability in a grooved heat pipe. Do *et al.* [6] developed a mathematical model which accurately predicted the thermal performance of a flat micro heat pipe with rectangular grooves. Ranjan *et al.* [7] developed a numerical model based on a static, evaporating film meniscus in various wick structures in heat pipes. A parametric study based on the effects of wall superheat, contact angle and wick porosity on evaporation rates was also conducted. In a related study [8], an effective thermal resistance for the conduction/evaporation process, from the bottom of wick structure to the saturated vapor, was proposed for a packed-sphere wicking structure. Zhao *et al.* [9] investigated the effect of temperature-dependent thermophysical properties on modeling the evaporating liquid meniscus in rectangular micro-channels. Cheng *et al.* [10] developed a mathematical model to determine heat transfer through both the thin-film and bulk regions of a liquid in a rectangular microgroove.

In the current investigation, a detailed mathematical model predicting the effect of the thin-film region on the evaporating heat transfer in a rectangular groove has been developed in order to find the maximum evaporating heat transport capacity through the thin-film region.

Film thickness and evaporation heat transfer in thin-film region

As shown in fig. 1, the axial flow in the rectangular groove can be divided into three stages [11-13], *i. e.*, the accommodation stage, the jump-like stage, and the corner flow stage.

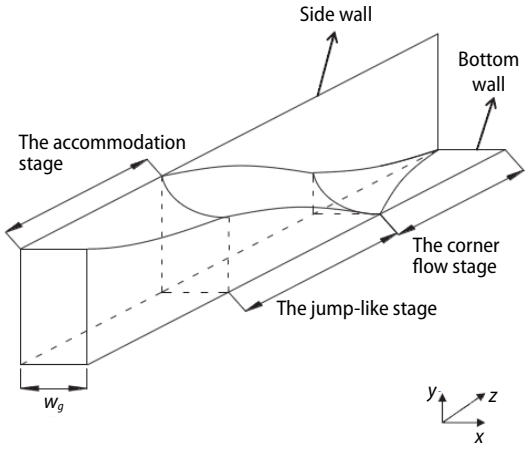

Figure 1. Schematic of axial flow along the rectangular microgroove

When heat is added on the bottom of the rectangular groove, the heat will transfer through the solid regions of groove wall and reach the working fluid. On 2-D cross-section of the microgroove, as shown in fig. 2, when the meniscus comes close to the side wall, the thin liquid film in the vicinity of the triple-phase contact line, which is defined as microregion in the paper, evaporates intensively. Most of the heat will transfer through thin-film regions. In the accommodation stage, the liquid film can be formed on the side wall of the microgroove with two extensive evaporating thin-film regions. At the jump-like stage, there are two intensive evaporating thin-films on the groove side walls: A-A and B-B regions in fig. 2(a), and due to the groove symmetry, the A–A thin--film region is the same as the B–B thin-film region; when the meniscus touches the bottom of the groove, there are not only two side thin-films: B-B region, but also two bottom thin-films: C-C region in fig. 2(b); at the stage of corner flow, each triangular zone has two intensive evaporating thin-films: B-B and C-C regions in fig. 2(c). Therefore, at different axial flow stage, the liquid film distribution on the cross-section is different, and the heat transfer characteristics are also different.

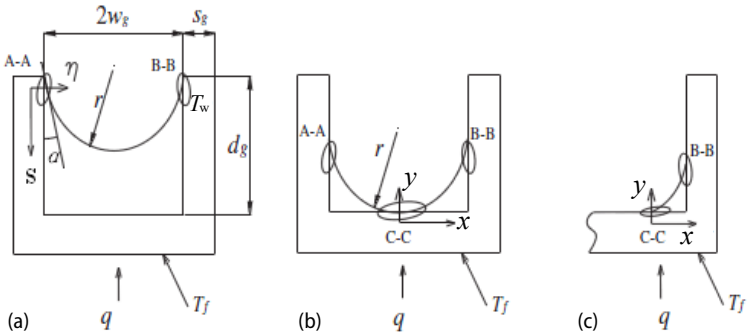

Figure 2. Liquid configuration on cross-section of the microgroove rectangular; (a) Beginning of the jump-like state, (b) end of the jump-like state, and (c) the corner flow state

For the thin-film evaporation heat transfer, the liquid-vapor interface temperatures on those thin-film regions can be depicted by the Clausius-Clapeyron equation [14, 15].

$$\left(\frac{\mathrm{d}p}{\mathrm{d}T}\right)_{\mathrm{sat}} = \frac{h_{fg}}{T_{\mathrm{sat}}\left(\frac{1}{\rho_{\mathrm{V}}} - \frac{1}{\rho_{\mathrm{L}}}\right)} \tag{1}$$

Integrating from the saturated temperature, T_{sat}, to the interface temperature, T_{LV}, results in a relationship between the interface temperature and the saturated vapor temperature, *i. e.*:

$$T_{\mathrm{LV}} = T_{\mathrm{V}}\left[1 + \frac{\Delta p}{\rho_{\mathrm{V}} h_{fg}}\right] \tag{2}$$

where can be found from:

$$\Delta p = \frac{\sigma}{r} + p_d \tag{3}$$

where the second term, p_d, in eq. (3) can be calculated by the equation developed by Holm and Goplen [16]:

$$p_d = \rho_L \mathrm{R}_{\mathrm{V}} T_{\mathrm{sat}} \ln(a\delta^b) \tag{4}$$

In the non-evaporating film region, the curvature effect can be neglected due to the absence of vaporization. The interface temperature at this region will be equal to the wall temperature due to the interface thermal resistance. Substituting eqs. (3) and (4) into eq. (2), the film thickness in this region can be obtained:

$$\delta_0 = \exp\left\{\left[\left(\frac{T_{\mathrm{W}}}{T_{\mathrm{sat}}} - 1\right)\left(/\frac{\rho_{\mathrm{V}} h_{fg}}{\rho_{\mathrm{L}} \mathrm{R}_{\mathrm{V}} T_{\mathrm{sat}}}\right) - \ln a\right] / b\right\} \tag{5}$$

Based on the geometry dimensions of the rectangular shape, the film thickness in A-A and B-B regions can be calculated:

$$\delta_{\text{A-A}} = \delta_{\text{B-B}} = w_g + \delta_0 - \sqrt{r^2 - (r\sin\alpha + s)^2} \tag{6}$$

$$\delta = \delta_0\,,\quad r \to \infty\,,\quad T_{\text{LV}} = T_{\text{W}}\quad \text{at}\quad s = 0$$

Based on the contact angle and dimensions shown in fig. 2, the meniscus radius can be written:

$$r = \frac{w_g}{\cos\alpha} \tag{7}$$

Based on the geometry dimensions of the rectangular shape and the definition of contact angle, the film thickness for both the C-C and D-D regions can be calculated:

$$\delta_{C-C} = r + \delta_0 - \sqrt{r^2 - x^2} \tag{8}$$

$$\delta = \delta_0\,,\quad r \to \infty\,,\quad T_{\text{LV}} = T_{\text{W}}\quad \text{at}\quad x = 0$$

The heat conduction through the thin liquid film is assumed normal to the wall of the groove. The extremely small thickness of the liquid layer in the evaporating thin-film region makes it necessary to consider the interfacial heat resistance. Then the heat flux through the thin liquid film can be written:

$$q_{\text{micro}} = \frac{T_{\text{W}} - T_{\text{LV}}}{\dfrac{\delta}{k_{\text{L}}} + \dfrac{R_i}{\sqrt{1 + \left(\dfrac{\text{d}\delta}{\text{d}s}\right)^2}}} \tag{9}$$

$$R_i = \frac{2-f}{2f}\frac{T_{\text{sat}}\sqrt{2\pi \text{R}_{\text{V}} T_{\text{sat}}}}{h_{fg}^2 \rho_{\text{V}}}\Delta V \tag{10}$$

So the heat flux through the thin liquid film can be expressed:

$$q_{\text{micro}} = \frac{T_{\text{W}} - T_{\text{LV}}}{\dfrac{\delta}{k_{\text{L}}} + \dfrac{T_{\text{sat}}\sqrt{2\pi \text{R}_{\text{V}} T_{\text{sat}}}}{h_{fg}^2 \rho_{\text{V}}}\dfrac{2-f}{2f}} \tag{11}$$

At the accommodation stage, the heat transfer through evaporating thin-films on 2-D cross-section of the microgroove can be calculated:

$$Q_{\text{micro1}} = 2\int_0^s q_{\text{mirco}}(s)\text{d}s \tag{12}$$

At the jump-like stage or the corner flow stage, there are four evaporating thin-films, the heat transfer through four thin-films can be calculated:

$$Q_{\text{micro2}} = 2\int_0^s q_{\text{mirco}}(s)\text{d}s + 2\int_0^x q_{\text{mirco}}(x)\text{d}x \tag{13}$$

Heat transfer through macroregion

Because the groove dimension as shown in fig. 2 is in a range of 0.2-0.4 mm and the Bond number is much less than 1, the temperature distribution in the macro-liquid film region can be described by the 2-D, steady-state heat conduction equation:

$$\frac{\partial^2 T}{\partial x^2} + \frac{\partial^2 T}{\partial y^2} = 0 \tag{14}$$

The solution for eq. (14) can be obtained by the FLUENT software, and the heat transfer through the macroregion can be obtained. The grid width near the evaporating thin-film is extremely small in order to improve calculation accuracy. In the macroregion, the effect of disjoining pressure on the interface temperature can be neglected. The liquid-vapor interface temperature in the macroregion can be determined:

$$T_{\mathrm{LV}} = T_{\mathrm{sat}}\left(1 + \frac{\sigma}{\rho_{\mathrm{V}} h_{fg}}\right) \tag{15}$$

Using eq. (15) for the liquid-vapor interface temperature, the heat transport Q_{macro} through the macroregion of liquid for a given superheat can be calculated. The total heat transport from the solid wall to the liquid can be determined:

$$Q_{\mathrm{tot}} = Q_{\mathrm{macro}} + Q_{\mathrm{micro}} \tag{16}$$

where Q_{micro} can be calculated by eq. (13) for a given superheat. During the iterative calculation, when the error is less than 0.1 W, the calculation is considered as the converged results.

Results and discussion

The disjoining pressure and interface curvature significantly influence the variation of film thickness, interface temperature, and heat flux distribution. In order to better illustrate effects on the meniscus radius, heat flux distribution and heat transport capacity, a rectangular groove, similar to the one shown in fig. 2, with dimensions of $w_{\mathrm{g}} = 0.000125$ m, $d_{\mathrm{g}} = 0.0005$ m, $s_{\mathrm{g}} = 0.0004$ m, and a groove number of 30, is considered. The thermophysical properties of borosilicate glass and pure saturated water at 60 ºC are utilized in the current investigation.

Figure 3 shows the influence of contact angle on the meniscus radius. As shown, it can be seen that the meniscus radius increases non-linearly with the improvement of contact angle. For example, when the contact angle changes from $\alpha = 0°$ to $\alpha = 45°$, the radius changes slowly and the ratio of the meniscus radius at $\alpha = 45°$ to the one at $\alpha = 0°$ is equal to 1.414, the ratio of the meniscus radius at $\alpha = 60°$ to the one at $\alpha = 45°$ is also equal to 1.414, while the ratio of the meniscus radius at $\alpha = 89°$ to the one $\alpha = 60°$ is 29.4. It shows that when the contact angle is less than 60°, the further decrease of the contact angle is not significantly further reduce the meniscus radius. When the contact angle is 90°, the meniscus radius tends to infinity.

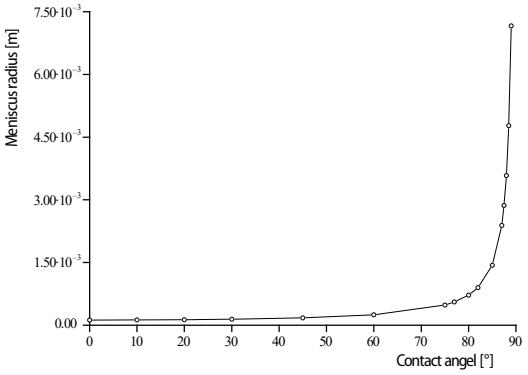

Figure 3. Meniscus radius *vs.* contact angle

Figures 4 and 5 show the influence of contact angle on thin-film thickness in A–A (or B–B) and C–C regions for rectangle microgroove, respectively. As shown, the thin-film thickness in the A–A (or B–B) thin-film region largely depends on the contact angle, while the thin-film thickness in the C–C thin-film region changes with the improvement of the contact angle insignificantly. The thin-film thickness in the A–A (or B–B) region almost increases linearly as the contact angle increases, while the thin-film thickness in the C–C region increases non-linearly with the improvement of contact angle. When the contact angle further increases, the thin-film thickness in the A–A (or B–B) region for rectangle microgroove increases very sharply. The difference is that the thin-film thickness in A–A (or B–B) region increases slowly along the s-direction when the contact angle is equal to zero.

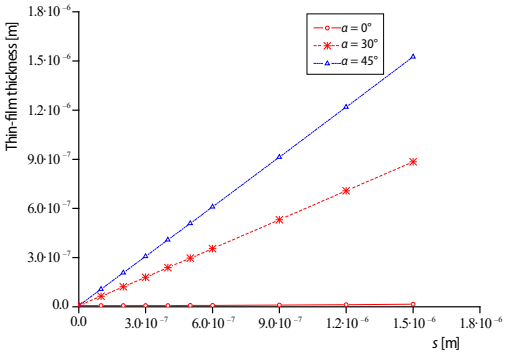

Figure 4. Meniscus radius *vs.* contact angle in A–A (or B–B) thin-film region

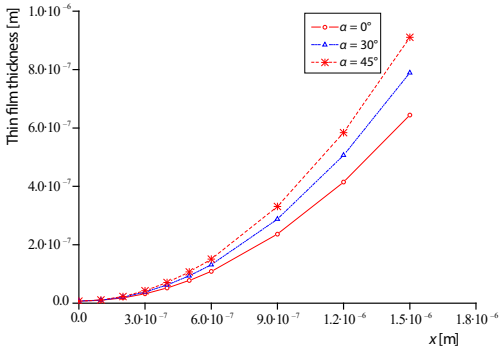

Figure 5. Meniscus radius *vs.* contact angle in C–C thin-film region

Figures 6 and 7 show the influence of contact angle on heat flux distribution in A–A (or B–B) and C–C thin-film regions for rectangle microgroove, respectively. As shown, the heat flux distribution in the A–A (or B–B) thin-film region largely depends on the contact angle, while heat flux distribution in the C–C region changes with the improvement of the contact angle insignificantly. The heat flux distribution in both A–A (or B–B) and C–C region increases non-linearly as the contact angle decreases. Although the highest heat flux is nearly the same, the total heat transfer through the thin-film region increases with the reduction of contact angle. Comparisons of the results shown in fig. 6 with those shown in fig. 7 indicate that the heat flux distributions in A–A (or B–B) and C–C regions for rectangle microgroove are similar. The initial heat fluxes in both regions are zero at the origin point where the film thickness is equal to δ_0, and then increase sharply with the improvement of film thickness. After reaching the maximum, the heat flux through the thin-film region almost decreases dramatically along the s- or x-direction. The difference is that the heat flux in A–A (or B–B) region decreases slowly along the s-direction when the contact angle is equal to zero.

Figures 8 and 9 show the influence of superheat on heat flux distribution in A–A (or B–B) and C–C thin-film regions at $\alpha = 30°$ for rectangle microgroove, respectively. As shown, the heat flux distributions in the A–A (or B–B) and C–C thin-film region largely depend on superheat. With the increase of temperature difference between groove wall and saturate vapor, the heat flux increases and the heat transfer through A–A, B–B, or C–C region enhances. The heat flux distributions in both A–A (or B–B) and C–C increase non-linearly as the contact angle decreases. Comparisons of the results shown in fig. 8 with those shown in fig. 9 indicate that the heat flux distributions in A–A (or B–B) and C–C regions for rectangle microgroove are

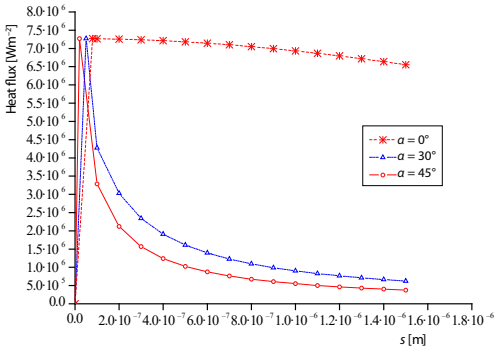

Figure 6. Contact angle effect on heat flux distribution in A–A or B–B thin-film region at $T_{superheat}$ = 1 K

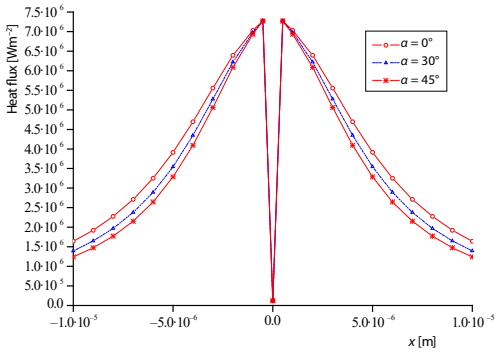

Figure 7. Contact angle effect on heat flux distributions in C–C thin-film region at $T_{superheat}$ = 1 K

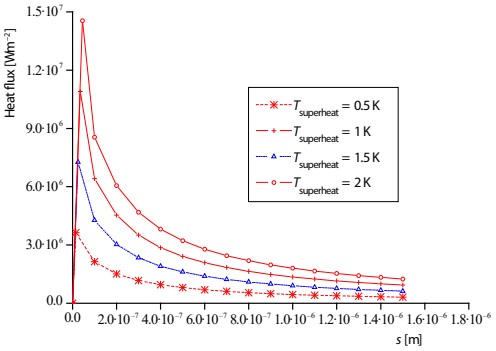

Figure 8. Superheat effect on the heat flux distribution in A–A or B–B thin-film region at α = 30°

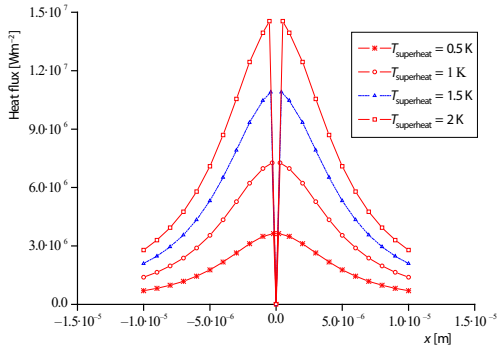

Figure 9. Superheat effect on heat flux distributions in C–C thin-film region at α = 30°

similar too. When the heat flux reaches the maximum, the heat flux through the thin-film region decreases dramatically along the s- or x-direction. The total heat transfer through the thin-film region increases with the improvement of superheat.

Figure 10 shows the influence of superheat on the ratio of the heat transfer through A–A (or B–B) thin-film region, Q_{micro}, to the total heat transfer, Q_{tot}. As shown, it can be seen that, with the increase of the superheat, the ratio decreases and it also depends on the contact angle. The main reason is that the thin-film region in A–A (or B–B) region has been extended and heat transfer through those regions enhances with the reduction of contact angle. When the contact angle is equal to zero, the heat transfer in the thin-film region accounts for more than 80% of the total heat transfer. The reason for high strength heat

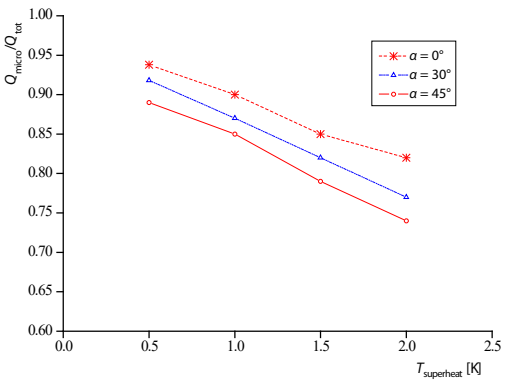

Figure 10. Contact angle effect on Q_{micro}/Q_{tot}

transfer in the thin-film region is the intensive evaporation in the rectangle capillary microgroove. With the increase of contact angle, the proportion of heat transfer in thin-film region decreases rapidly. Therefore, the liquid with high wetting performance is more capable of playing the advantages of higher intensity heat transfer in thin-film region.

Conclusions

Physical and mathematical models predicting the effects of contact angle and superheat on the thin-film profile for a rectangle microgroove have been developed. The main conclusions are as follows.

- The meniscus radius increases non-linearly with the improvement of contact angle. When the contact angle in a rectangle microgroove is less than 60°, the further decrease of the contact angle is not significantly further reduce the meniscus radius. When the contact angle is 90°, the meniscus radius tends to infinity.
- The thin-film thickness in the A–A (or B–B) thin-film region largely depends on the contact angle, while the thin-film thickness in the C–C thin-film region changes with the improvement of the contact angle insignificantly. The thin-film thickness in the A–A (or B–B) region almost increases linearly as the contact angle increases, while the thin-film thickness in the C–C region increases non-linearly with the improvement of contact angle. When the contact angle further increases, the thin-film thickness in the A–A (or B–B) region for rectangle microgroove increases very sharply. The difference is that the thin-film thickness in A–A (or B–B) region increases slowly along the s-direction when the contact angle is equal to zero.
- The heat flux distribution in the A–A (or B–B) thin-film region largely depends on the contact angle, while heat flux distribution in the C–C region changes with the improvement of the contact angle insignificantly. The heat flux distribution in both A–A (or B–B) and C–C region increases non-linearly as the contact angle decreases. The difference is that the heat flux in A–A (or B–B) region decreases slowly along the s-direction when the contact angle is equal to zero.
- The heat flux distributions in the A–A (or B–B) and C–C thin-film region largely depend on superheat. With the increase of temperature difference between groove wall and saturate vapor, the heat flux increases and the heat transfer through A–A, B–B or C–C region enhances.
- The total heat transfer through the thin-film region increases with the improvement of superheat, and decreases as the contact angle increases. When the contact angle is equal to zero, the heat transfer in the thin-film region accounts for more than 80% of the total heat transfer. Intensive evaporation in the thin-film region plays a key role in heat transfer for the rectangle capillary microgroove. The liquid with high wetting performance is more capable of playing the advantages of higher intensity heat transfer in thin-film region.

Acknowledgment

The authors acknowledge the financial support provided by National Natural Science Foundation of China (Grant No. 51476172) and the Fundamental Research Funds for the Central Universities (2018yz02).

Nomenclature

a – constant, (= 1.5787)
b – constant, (= 0.0243)
d_g – depth of microgroove, [m]
f – evaporation coefficient
h_{fg} – latent heat, [Jkg^{-1}]
k – conductivity, [Wm^{-1}K^{-1}]
p – pressure, [Pa]
Q – heat transfer, [W]
q – heat flux, [Wm^{-2}]
R_i – interfacial heat resistance, [m^{2}KW^{-1}]

R_V – specific gas constant, [Jkg^{-1}K^{-1}]
r – curvature radius of the meniscus, [m]
s_g,s – spacing of microgroove, [m]
T – temperature, [K]
w_g – half width of microgroove, [m]

Greek symbols

α – contact angle between the liquid and the groove wall
δ – thickness of the liquid film, [m]
δ_0 – initial thickness of the evaporating thin-film, [m]
ρ – density, [kgm^{-3}]
σ – coefficient of surface tension, [Nm^{-1}]

Subscripts

A–A – thin-film region in fig. 2
B–B – thin-film region in fig. 2
C–C – thin-film region in fig. 2
d – disjoining
L – liquid
LV – liquid-vapor interface
macro – macroregion
micro – micro region
sat – saturated
tot – total
V – vapor
W – wall

References

[1] Ma, H. B., *et al*., Fluid Flow and Heat Transfer in the Evaporating Thin-film Region, *Microfluidics and Nanofluidics*, *4* (2008), 3, pp. 237-243
[2] Yan, C. J., Ma, H. B., Analytical Solutions of Heat Transfer and Film Thickness in Thin-Film Evaporation, *Journal of Heat Transfer*, *135* (2013), 5, pp. 1-6
[3] Jiao, A. J., *et al*., Thin Film Evaporation Effect on Heat Transport Capability in a Grooved Heat Pipe, *Microfluidics and Nanofluidics*, *1* (2005), 3, pp. 227-233
[4] Li, C., *et al*., Evaporation/Boiling in Thin Capillary Wicks (I): Wick Thickness Effects, *Journal of Heat Transfer*, *128* (2006), 12, pp. 1312-1319
[5] Jiao, A. J., *et al*., Evaporation Heat Transfer Characteristics of a Grooved Heat Pipe with Micro-Trapezoidal Grooves, *International Journal of Heat and Mass Transfer, 50* (2007), 15-16, pp. 2905-2911
[6] Do, K. H., *et al*., A Mathematical Model for Analyzing the Thermal Characteristics of a Flat Micro Heat Pipe with a Grooved Wick, *International Journal of Heat and Mass Transfer*, *51* (2008), 19-20, pp. 4637-4650
[7] Ranjan, R., *et al*., Analysis of the Wicking and Thin-Film Evaporation Characteristics of Microstructures, *Journal of Heat Transfer*, *131* (2009), 10, pp. 1-11
[8] Ranjan, R., *et al*., A Microscale Model for Thin-Film Evaporation in Capillary Wick Structures, *International Journal of Heat and Mass Transfer*, *54* (2011), 1-3, pp. 169-179
[9] Zhao, J. J., *et al*., Effects of Superheat and Temperature-Dependent Thermophysical Properties on Evaporating Thin Liquid Films in Microchannels, *International Journal of Heat and Mass Transfer*, *54* (2011), 5-6, pp. 1259-1267
[10] Cheng, P., *et al*., Heat Transfer in Bulk and Thin-Film Fluid Regions of Rectangular Microgroove, *Journal of Thermophysics and Heat Transfer*, *26* (2012), 1, pp. 108-114
[11] Nilson, R. H., *et al*., Steady Evaporating Flow in Rectangular Microchannels, *International Journal of Heat and Mass Transfer*, *49* (2006), 9-10, pp. 1603-1618
[12] Guo, C. H., *et al*., Effect of Mechanical Vibration on Flow and Heat Transfer Characteristics in Rectangular Microgrooves, *Applied Thermal Engineering*, *52* (2013), 52, pp. 385-393
[13] Guo, C. H., *et al*., Analysis on Cross Sectional Heat Transfer Characteristics in Rectangular Microgrooves, *Journal of Engineering Thermophysics*, *32* (2011), 7, pp. 1169-1172
[14] Wayner, P. C., *et al*., The Interline Heat Transfer Coefficient of an Evaporation Wetting Film, *International Journal of Heat and Mass Transfer*, *19* (1976), 5, pp. 487-492
[15] Wayner, P. C., Adsorption and Capillary Condensation at the Contact Line in Change of Phase Heat Transfer, *International Journal of Heat and Mass Transfer*, *25* (1982), 5, pp. 707-713
[16] Holm, F. W., Goplen, S. P., Heat Transfer in the Meniscus Thin Film Transition Region, *ASME Journal of Heat Transfer*, *101* (1979), 3, pp. 543-547

Paper submitted: January 14, 2016
Paper revised: October 20, 2016
Paper accepted: October 25, 2016